Since January 2020 Elsevier has created a COVID-19 resource centre with free information in English and Mandarin on the novel coronavirus COVID-19. The COVID-19 resource centre is hosted on Elsevier Connect, the company's public news and information website.

Journal of Molecular Structure 1221 (2020) 128869

Contents lists available at ScienceDirect

Journal of Molecular Structure

journal homepage: www.elsevier.com/locate/molstr

Structural basis of quinolone derivatives, inhibition of type I and II topoisomerases and inquiry into the relevance of bioactivity in odd or even branches with molecular docking study

Yilin Wang[a], Fuyan Xiao[b], Guofan Jin[b,*]

[a] The People's Hospital of Danyang, Affiliated Danyang Hospital of Nantong University, Zhenjiang, 212300, PR China
[b] School of Pharmacy, Jiangsu University, Zhenjiang 212013, PR China

ARTICLE INFO

Article history:
Received 18 May 2020
Revised 8 July 2020
Accepted 9 July 2020
Available online 9 July 2020

Keywords:
Molecular docking
Structure–activity relationship
Quinolinium iodide
Anticancer agents
Antibacterial agents

ABSTRACT

The structural modification of quinolone derivatives has been a hot spot in recent years, especially the modification of the N-1 position, which is the part that this article focuses on. In this paper, series of synthesized quinoline quaternary ammonium salts with odd and even carbon number alkyl groups in N-1 position were used to explain the influence of the alkyl side chain on activity. With respect to all the recently synthesized twenty products, the biological activity results exhibited significant antitumor and antibacterial activity with obvious differences in the target alkyliodine substituted compounds and the antibacterial activities apparently had the prominent odd-carbon number predominance. Compound 8-((4-(benzyloxy)phenyl)amino)-7-(ethoxycarbonyl)-5-propyl-[1,3]dioxolo[4,5-g]quinolin-5-ium (**4d**) was found to be the most potent derivative with IC_{50} values of 4 ± 0.88, 4 ± 0.42, 14±1.96, and 32±3.66 against A-549, Hela, SGC-7901, and L-02 cells, respectively, stronger than the positive control 5-FU and MTX. Furthermore, it had the most potent bacterial inhibitory activity of MIC value against E. coli (ATCC 29213) and Staphylococcus aureus (ATCC 8739) at 3.125 nmol mL^{-1}. With respect to molecular simulations, in order to illustrate the possible mechanism of the difference between the series of compounds in the even or odd carbon chain alkyliodine substitution, this paper simulated the conceivable mode and explained the main interactions. Finally, we could find that the position and proportion of hydrogen bonds and other interactions in each series were regarded as the main reasons for this difference in activity.

1. Introduction

As an important antibacterial agent, quinolone has been widely concerned by human beings. As a fully synthetic drug, quinolone drugs have also played a great role in the field of antibacterial and anticancer [1–3]. Since the first synthetic quinolone drug was put into clinical practice in 1962, this family has a history of nearly 60 years, and it has indeed become a veteran role of antibacterial drugs [4–8]. The most primitive discoveries often give people infinite enlightenment, guide future generations to design and synthesize based on this drug and have had very successful cases, but also stimulated experts to explore their molecular level mechanism of action [9–14]. For the design and development of any pharmacy, relevant internal mechanism research is often indispensable [15–25]. As of now, it is well known that the target of quinolone drugs is topoisomerase, and the target of antibacterial action is topoisomerase II. The main mechanism of its anticancer activity has recently been discovered as an inhibitor of topoisomerase I [5,26,27]. DNA topoisomerase plays an important role in the regulation of DNA transcription, replication and gene expression. Studies have found that DNA topoisomerases in cancer cells exhibit high levels of expression independent of other factors. Quinolone derivatives exhibit cytotoxicity by intercalating DNA and thus interfere with the DNA replication process, and have achieved initial success in drug design. For example, some anticancer agents based on topoisomerase I have been launched in the early 21st century. Belotecan hydrochloride, led by Chong KunDang, has shown outstanding advantages for the treatment of non-small cell lung cancer and ovarian cancer. The latter irinotecan hydrochloride developed by Yakult and Pfizer has emerged in the fight against the small cell lung cancer, gastric cancer and solid cancer. Amaridine is another marketed anticancer drug targeted at topoisomerase II, which is used in the treatment of leukemia. [28–31] After the exploration of experts, quinolones exert their biological activities by inhibiting the formation of bacterial DNA topoisomerase. The successful exploration of

* Corresponding author.
E-mail address: 1000004770@ujs.edu.cn (G. Jin).

https://doi.org/10.1016/j.molstruc.2020.128869
0022-2860/

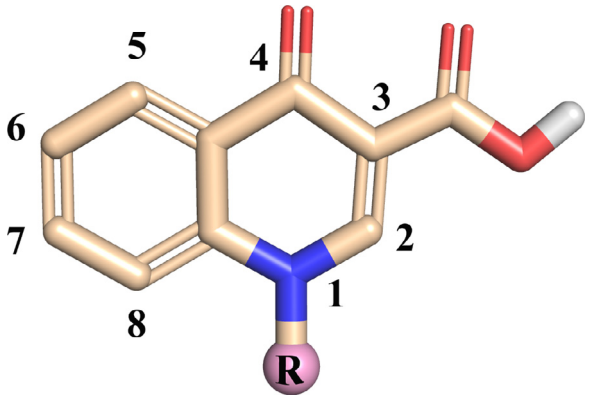

Fig. 1. The parent structure of fluoroquinolones.

this mechanism provides the basis for the subsequent drug design. Drug designers no longer hunted around like a headless chicken, and since then quinolone drug design has a real design center [32–34].

During the treatment of COVID-19, meantime, the chloroquine compound with quinolone nucleus has also become a major research direction for new drugs [35–37]. This drug has always existed as a mature antimalarial drug with known toxic and side effects, and the treatment in this outbreak has also played a special role, allowing experts to see the hope of treatment. Due to its good performance, numerous structural modifications of quinolone core to optimize the activity have become the critical project [38–42]. The modifications mainly occur at 1-position and 4-position (Fig. 1). Among these options, the structure modification of the quaternary amine in N-1 position optimizes its antibacterial activity and give the dual anticancer and antibacterial activities [43–48]. The quaternary ammonium salt contains an ionized nitrogen atom as an important sign [49]. It has also been active in the eyes of researchers with the role of disinfection and antibacterial agents.

Quaternary ammonium salts can be used in surfactants (materials field), disinfection and antibacterial agents (biomedical field), and so on. They are widely used as fabric conditioners, fabric softeners, insecticides, plant growth promoters, etc. In the disinfectant and bactericide industry, quaternary ammonium salts have also been adopted by the market as excellent disinfectants. For example, in the process of COVID-19 epidemic prevention and control, they have also played an important role in eliminating viruses. From the above considerations, the combination of both quinolone and quaternary ammonium salt can effectively promote the activity. However, the alkyl carbon number of the quaternary ammonium salt also becomes an important factor affecting the activity.

This article summarized the published papers and summarizes the effects of the carbon chain odd and even carbon effects in the quaternary ammonium salt group. At the same time, a series of quinolone quaternary ammonium salt compounds combined by this subject were used for auxiliary verification. Through the biological activity (anticancer and antibacterial) test of all target products, the results were combed to draw a staged conclusion, and molecular simulations were also used to explain the possible mechanism.

2. Modification of quinolone N-1 position

Due to its good antibacterial activity and convenient oral administration, quinolone drugs have always occupied an important position in synthetic drugs. At the same time, with the research on structure-activity relationship in recent years, the research value of this class of synthetic drugs has also greatly increased. Common structural modifications are mainly inclined to increase antibacterial activity. In recent years, more and more quinolone drugs have been used in the development of anticancer drugs, such as dini. The common modification group is an alkyl substituent, and the salt-forming structure modification at the N-1 position also shows a good effect on the modification (Scheme 1). Studies have shown that the antibacterial activity of quinolone may be determined by two factors, one is the drug's ability to inhibit the target enzyme DNA gyrase, the other is the transport effect or post-rotation process [50–57]. Therefore, it may lead to erroneous conclusions based on the traditional minimum inhibitory concentration (MIC) without considering target enzyme factors [58–62]. This paper reports the effects of the systematic changes of R^1 salt-forming groups (20 compounds) on the inhibitory effects of bacterial and cancer cell growth. At the same time, the structure-activity relationship including the N-1 position is defined as far as possible synthesis of the best compounds and their activity as long as docking study of DNA topoisomerase.

2.1. Hydrocarbyl substitution

The quinolone structural modifications that generally occured at the N-1 position are mainly ethyl and cyclopropyl. Studies have found that bulky alkyl substituents have stronger antibacterial activity. 1 and 8 position can form a ring at the same time and it was also a common structural modification.

2.2. Quaternary ammonium salt modification

With the development of synthetic drugs, in order to improve the water solubility of drugs, the introduction of iodoalkyl at the N-1 position to form a quaternary ammonium salt structure has also become a new research direction. The parent body with antibacterial activity is modified by the quaternary ammonium salt structure to improve the water solubility of the target product. After this modification, the oil-water partition coefficient is improved in a reasonable direction.

3. Effects of salt formation at N-1 on biological activity

The introduction of alkyl chains through haloalkyl can achieve high efficiency and convenience [63,64]. In this paper, iodomethane, iodopropane, and iodoisopropane were used to grow and modify the N-1 chain to form salts, and a series of quinoline ammonium salts with odd carbon number chains were obtained (Scheme 2). The quaternary ammonium salt with even representative carbon chain is mainly synthesized from the derivatives of iodoethane and quinoline.

4. Methods and methodology

4.1. Biological activity

4.1.1. Antibacterial activity test

The synthesized MIC values of final compounds 1–20 were evaluated for their antibacterial activity against *E. coli* (ATCC 29213) and *Staphylococcus aureus* (ATCC 8739). The DMSO solution of test compounds were added to the culture medium to obtain final concentrations of 1–50 nmol mL^{-1}. A standardized suspension of the test bacterium was inoculated and incubated for 24–48 h at 37 °C, then the minimal inhibitory concentrations (MIC values) were calculated. In order to avoid random errors and ensure the accuracy of the experiment, we choose ciprofloxacin and amoxicillin as the controls and performed triple parallel experiments.

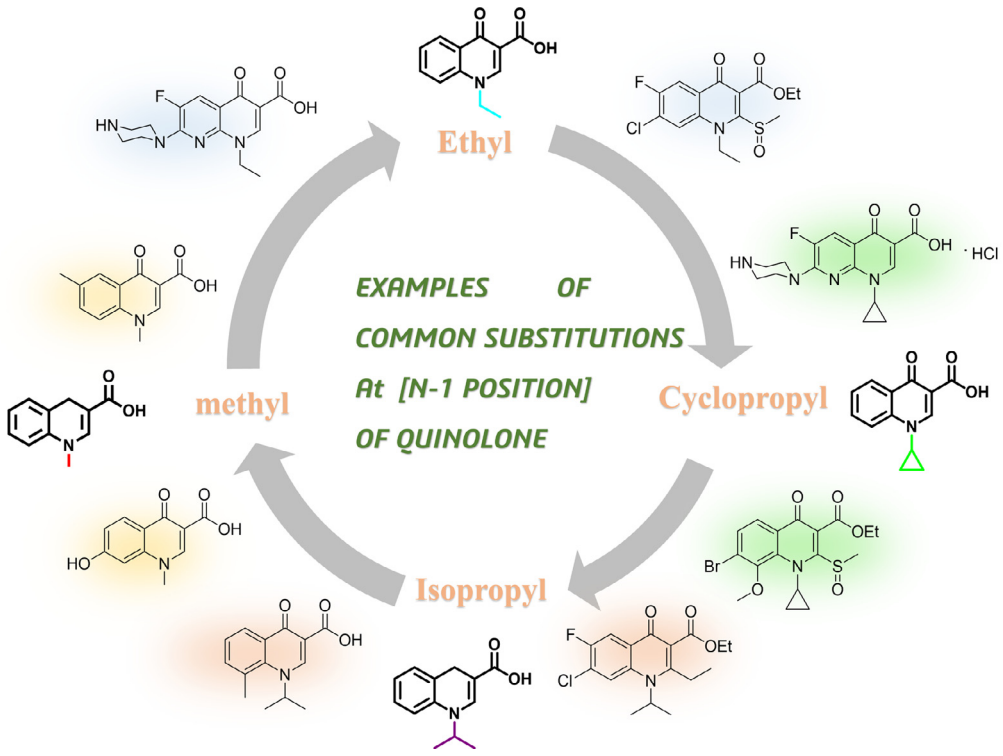

Scheme 1. Examples of common substitutions at the N-1 position of quinolone.

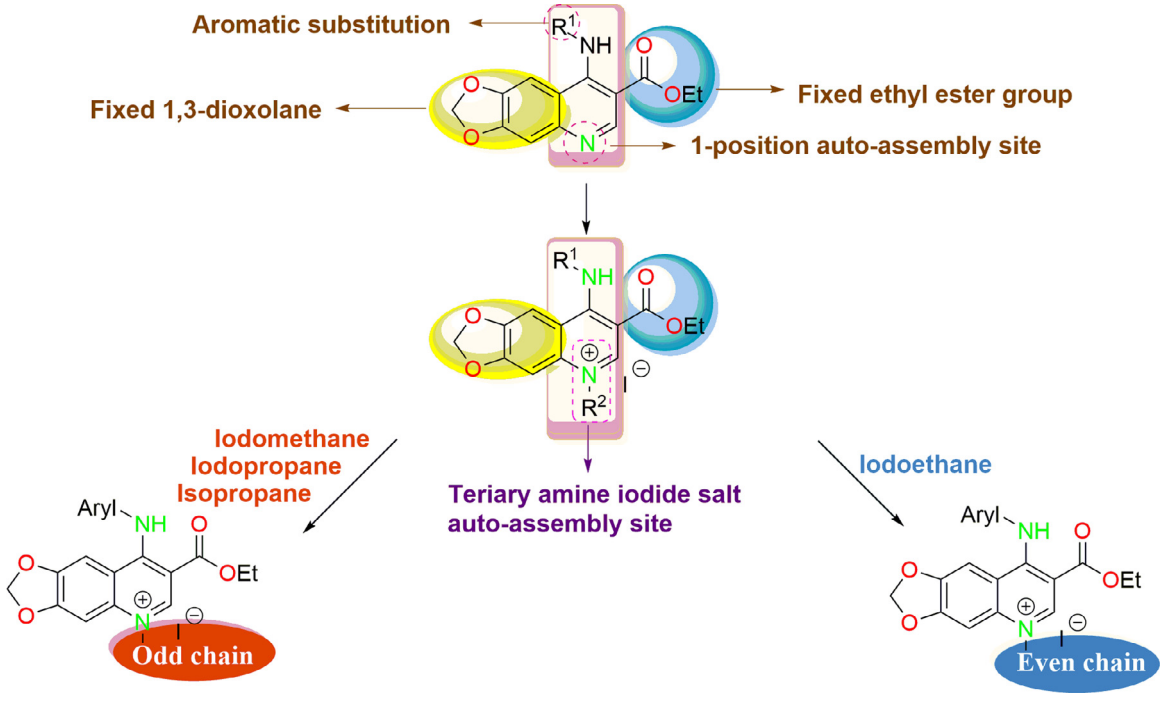

Scheme 2. Schematic diagram of overall design of synthesized active derivatives.

4.1.2. Cytotoxicity activity test

The human lung cancer cell line (A549), human Hela cell line (HeLa), human gastric cancer cell line (SGC-7901), and normal liver cell line (L-02) were used to evaluate the anti-proliferation of compounds in five cell lines active. Anticancer drugs were jointly tested for 5-FU and MTX as positive controls. Dissolved in DMSO and then performed activity tests.

4.2. Docking simulations

AutoDock Vina 1.1.2. and MGLTools software were used to perform docking simulations. In the present study, the 3D crystal structure of human topoisomerase I and *S. aureus* DNA gyrase (Topo II) reported in Protein Data Bank (PDB) were used as the receptor for docking studies (PDB ID: 1TL8, 2XCT). The co-crystallized

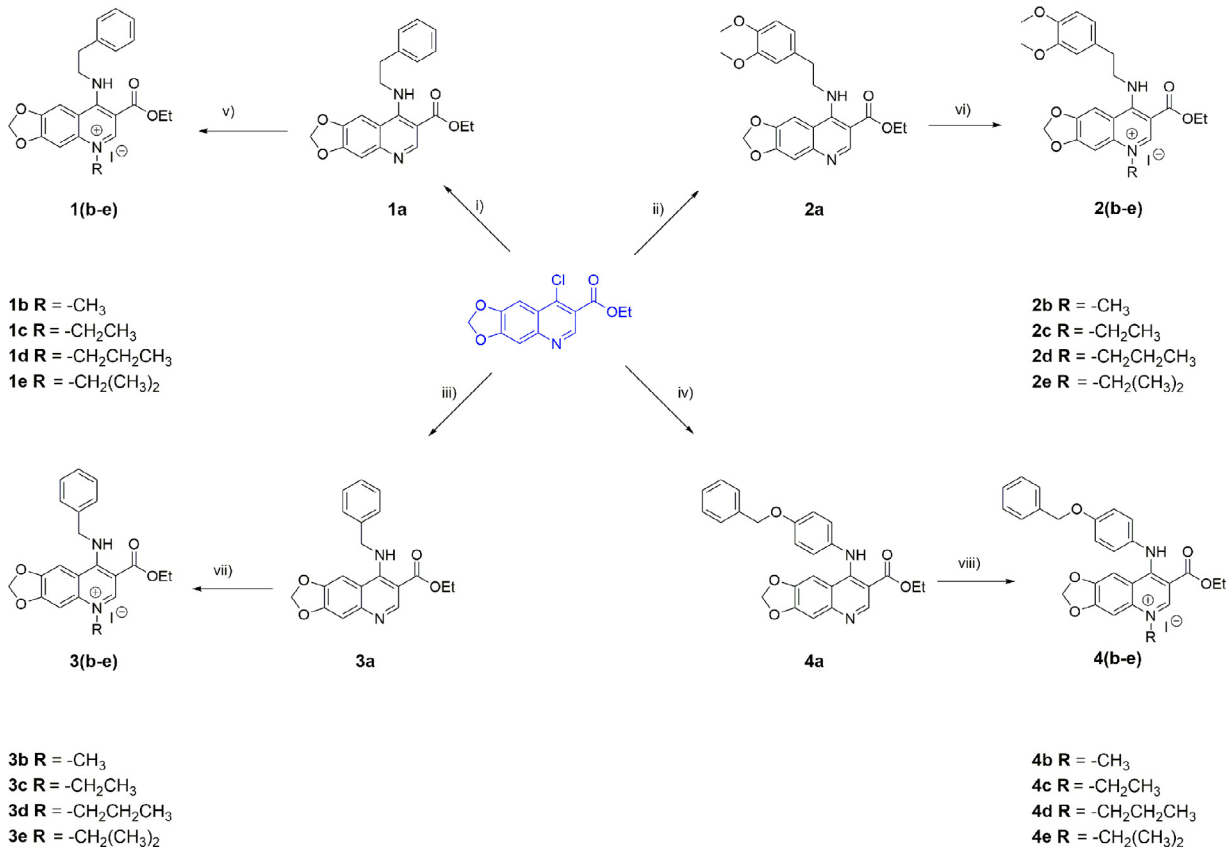

Scheme 3. The basic route for the synthesis of the target compound to be tested. Reagents and conditions: i) Phenethylamine, K_2CO_3, ACN, 80 °C, 8 h. ii) 3,4-Dimethoxyphenethylamine, K_2CO_3, ACN, 80 °C, 8 h. iii) Benzylamine, K_2CO_3, ACN, 80 °C, 8 h. iv) 4-Benzyloxyaniline hydrochloride, K_2CO_3, ACN, 80 °C, 8 h. v) R-I (Iodomethane (**1b**), Iodoethane (**1c**), 1-Iodopropane (**1d**), 2-Iodopropane (**1e**)), ACN, reflux, 2 h. vi) R-I (Iodomethane (**2b**), Iodoethane (**2c**), 1-Iodopropane (**2d**), 2-Iodopropane (**2e**)), ACN, reflux, 2 h. vii) R-I (Iodomethane (**3b**), Iodoethane (**3c**), 1-Iodopropane (**3d**), 2-Iodopropane (**3e**)), ACN, reflux, 2 h. viii) R-I (Iodomethane (**4b**), Iodoethane (**4c**), 1-Iodopropane (**4d**), 2-Iodopropane (**4e**)), ACN, reflux, 2 h.

structures of the target proteins were downloaded from the PDB and prepared for docking using the docking program AutoDockVina 1.1.2. and MGLTools. The docking result was analyzed and optimized by Pymol 1.5.6.

5. Result and discussion

5.1. Chemistry

We firstly synthesized series of ethyl-8-chloro-[1,3]dioxolo[4,5-g]quinoline-7-carboxylate intermediate. Then it was found that the synthetic route shown in Scheme 2, adapted from some related synthetic manipulations, could served as a suitable approach for the desired correspondence compounds. Subsequent synthetic studied revealed that the novel 7-(ethoxycarbonyl)−8-(arylamino)-[1,3]dioxolo[4,5-g]quinolin-5-ium iodide derivatives synthesized according to Scheme-3 could be obtained in moderate yield. The iodination of ethyl 8-(aryl)-[1,3]dioxolo[4,5-g]quinolone -7-carboxylate derivatives with an excess of iodomethane or iodopropane under reflux provided the target compounds (Scheme 3). Finally, we elucidated the bioactivity of target compounds from molecular docking study as having anticancer and antitumor activities.

5.2. The spectroscopic property of tested compounds

Ultraviolet-visible (UV–vis) spectra were recorded on a UV-2550 spectrophotometer using a 1 cm path length quartz cuvette at room temperature. Spectroscopic evaluation was performed in DMSO solvent at the concentration of 5 mM. It was found that the compounds in each series have spectral images with almost uniform absorption wavelengths, which may be caused by similar conjugated environments. Therefore, the compound in which methyl iodide is substituted as the representative is shown in Fig. 2. From the result, it is with characteristic benzene ring band that absorption in the wavelength region of 230–270 nm. The absorption peaks of the 1–3 series of spectra substituted with a benzene ring at the 4-position are located at 358 nm. The compound **4b** with bisbenzene ring substitution has a peak at 380 nm that is different from several other products, which may be caused by the existence of a new conjugated environment between the C-4 benzyloxybenzene structure.

5.3. Evaluation of antibacterial activity in vitro

The antibacterial activity test was also possessed against *E. coli* (ATCC 29213) and *Staphylococcus aureus* (ATCC 8739) as shown in Table 1 and Fig. 3. Among the tested compounds **1a**-**4e** with the different 4-position N-phenyl substituent on quinoline possessed the changed dual activity against all cancer cell and strains tested.

In the respective series where each 4-position is the same, a parallel comparison under the condition against *S. aureus* (ATCC 8739) found that the compounds **1b, 1e, 2b, 2e, 3b, 3e** showed lower IC_{50} values. Compounds **3b** and **4b** showed 8 to 4 times the antibacterial activity compared to the reference variable, which was likely to be due to the salt-forming modification of the compound at N-1 position. This may be because the 1-position is substituted with an odd-chain alkyl chain. It is worth mentioning that

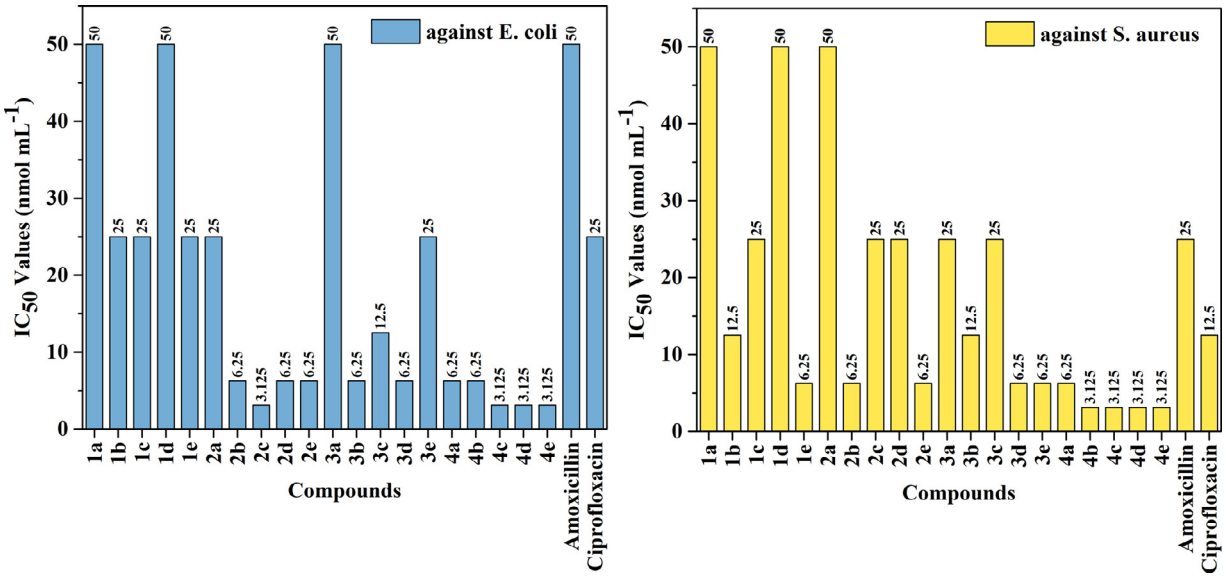

Fig. 2. Absorption spectra of (**1**–**4**) **b** in DMSO (concentration: 5 mM) at room temperature.

Table 1
Antibacterial screening in terms of the MIC (nmol mL^{-1}) for the tested compounds in reference to Ampicillin and Ciprofloxacin, respectively [63,64].

Compounds			MIC[a] / (nmol mL^{-1})		ClogP[b]
	R^1	R^2	*E. coli*	*S. aureus*	
1a	CH_2CH_2Ph	–	> 50	> 50	2.53
1b	CH_2CH_2Ph	CH_3	25	12.5	2.27
1c	CH_2CH_2Ph	CH_2CH_3	25	25	2.43
1d	CH_2CH_2Ph	$CH_2CH_2CH_3$	50	50	2.89
1e	CH_2CH_2Ph	$CH_2(CH_3)_2$	25	6.25	3.13
2a	$CH_2CH_2Ph(OCH_3)_2$	–	25	50	1.56
2b	$CH_2CH_2Ph(OCH_3)_2$	CH_3	6.25	6.25	1.22
2c	$CH_2CH_2Ph(OCH_3)_2$	CH_2CH_3	3.125	25	1.20
2d	$CH_2CH_2Ph(OCH_3)_2$	$CH_2CH_2CH_3$	6.25	25	2.11
2e	$CH_2CH_2Ph(OCH_3)_2$	$CH_2(CH_3)_2$	6.25	6.25	2.58
3a	CH_2Ph	–	> 50	25	2.18
3b	CH_2Ph	CH_3	6.25	12.5	1.97
3c	CH_2Ph	$-CH_2CH_3$	12.5	25	2.02
3d	CH_2Ph	$CH_2CH_2CH_3$	6.25	6.25	2.85
3e	CH_2Ph	$CH_2(CH_3)_2$	25	6.25	3.26
4a	$PhOCH_2Ph$	–	6.25	6.25	2.09
4b	$PhOCH_2Ph$	CH_3	6.25	3.125	1.88
4c	$PhOCH_2Ph$	CH_2CH_3	3.125	3.125	2.04
4d	$PhOCH_2Ph$	$CH_2CH_2CH_3$	3.125	3.125	2.67
4e	$PhOCH_2Ph$	$CH_2(CH_3)_2$	3.125	3.125	2.83
Amoxicillin	–	–	50	25	–
Ciprofloxacin	–	–	25	12.5	–

[a] MIC (minimum inhibitory concentration) values represent the average of three readings.
[b] calculated on ACD/Labs website.

the even-numbered branch substitution in series 3 gave compound **3c** the worst activity in this group at 25 nmol mL^{-1}, which extremely maybe due to the iodoethyl group substitution modification at the N-1 position. For series 4, when substituted by benzyloxyphenethylamine, the four alkyl substitutions all show the same activity intensity at 3.125 nmol mL^{-1} far exceeds the reference drug concentration of 25 nmol mL^{-1} in Amoxicillin and 12.5 nmol mL^{-1} in Ciprofloxacin of saccharin is probably because the aromatic hydrophobic structure of the large group at position 4 has a greater influence on antibacterial activity, temporarily exceeding the effect of the alkyl side chain. An overview of the overall biological activity presents an activity advantage of odd carbon number substitution.

At the same time, the ClogP value of the compound reflects the water solubility of the drug, which has special significance for whether the drug can penetrate the cell membrane and enter the cell to play a role. Compounds tend to be more water-soluble after salt formation, but this is also affected by the size of the salt-forming side chain groups. We can find that the volume of the iodoalkyl group with a 1-position substituent exhibits different ClogP values. For example, the formation of the quaternary ammonium salt of compound **1b** (methy iodine, logP = 2.27) increases the water solubility, which decreases slightly with the increase in branching until the effect of products **1e** (isopropyl iodine, logP = 3.13) was worse than the raw material **1a** (unsustitution, logP = 2.53), which also led the difference in activity.

5.4. Evaluation of cytotoxicity activity in vitro

The conversion of a 4-position carbonyl group to a hydrophobic aromatic amine group to obtain target compounds, and most of these structures contained a hydrophobic group, and then

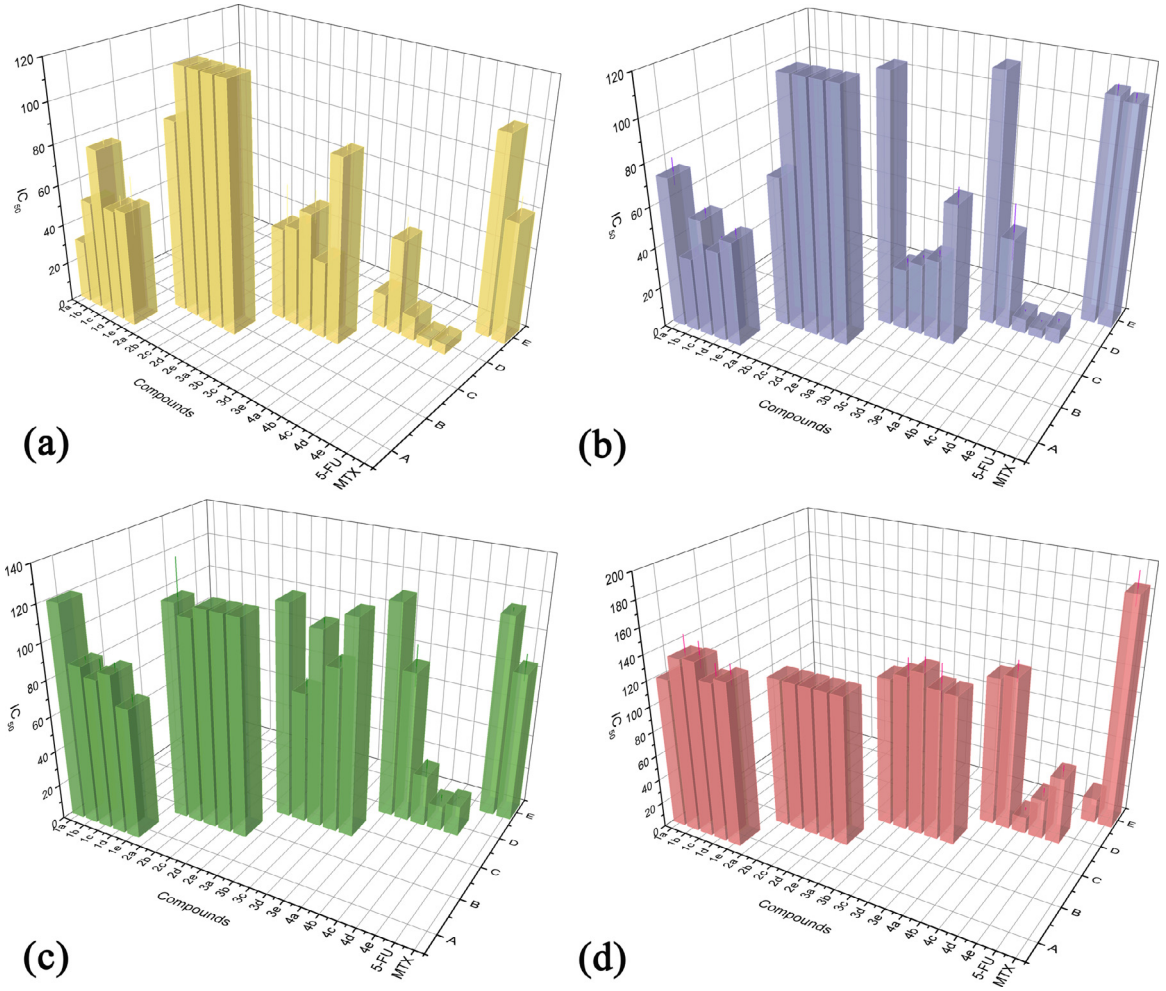

Fig. 3. Antibacterial screening in terms of the MIC (nmol mL^{-1}) for the tested compounds against *E. coli* and *S. aureus* in reference to Ampicillin and Ciprofloxacin, respectively.

quaternized ammonium salt at the N-1 position to form the final product. IC_{50} were assessed for their anti-proliferative activity in above mentioned five cell lines by MTT (3-(4,5-dimethylthiazol-2-yl) −2,5-diphenyltetrazolium bromide) assay (Fig. 4, Table 2). Compared with the positive control 5-FU and MTX, all 20 compounds showed superior anticancer activity. It is worth mentioning that the substitution of even-numbered carbon chains into salts shows unusual anticancer activity in each series against five cell lines. As shown in the activity experiments (Table 2), the anticancer activity (IC_{50}) of the products with even carbon chain substitution (such as compounds **1**–**4c**) were slightly inferior to other products with odd carbon chain in the same series of structurally modified quaternary ammonium salts at the 4-position. That is, among the quinoline compounds with same substituent at the 4-position, the anti-cell proliferation activity of the derivative substituted with the iodoethyl at the 1-position was weaker than that of the iodomethyl, iodopropyl, iodopropyl substituted products. For example, compounds **4d** of 4 ± 0.42~14±1.96 and **4e** of 5 ± 0.64~17±0.41 were 2~3 times more active than **4c** of 7 ± 0.48~29±5.79 against five cell lines.

5.5. Analysis of docking result

Molecular docking is an intuitive method that initially simulates the binding of compounds to sites of action. These tight interactions allow it to bind strongly to Topoisomerase II, which is considered a target for quinoline antibacterial effects. Therefore, the combination model clarifies the reason for the obvious efficacy of these compounds from another perspective. It was of interest to elucidate the mechanism by which the synthesized active compounds persuaded their antibacterial activities (Figs. 5–8). The co-crystallized structures of the target proteins of *S. aureus* were downloaded from the PDB bank and prepared for docking by AutoDockVina 1.1.2. and MGLTools (PDB ID: 2XCT). In the analysis of the molecule simulation results of antibacterial activity, in order to control the variables, we selected series 1 (**1a**-**1e**) and series 3 (**3a**–**3e**) with the same phenylethylamine substitution at the 4-position substituent for parallel comparison within each group (Figs. 5, 7). The 3D ligand interactions of the compound **1b** inhibitor with protein displayed affinity score −9.9 Kcal mol^{-1} and mainly showed two hydrogen bond acceptor interactions between N at 4-position of quinoline ring and bases DA 13 and DT 8 and ionic interactions between oxygen of the carbonyl group and amino acid residues D 437 and R 458. It also displayed Ar-H interaction with bases DT 10 and DA 13 along with π-π stacks between benzene substituent at 4-position and base DT 8 and DG 9, in addition to other hydrophobic interactions (Fig. 5a). Whereas the binding energies of compounds **1c** and **1d** were inferior to those of the same series of compounds, which are −8.7 and −8.9 Kcal mol^{-1}, respectively. There were no hydrogen bond interactions in compound **1c** binding mode. It exhibited Ar-Pi interactions between benzene ring of quinoline ring and base DT 10, with pyridine ring

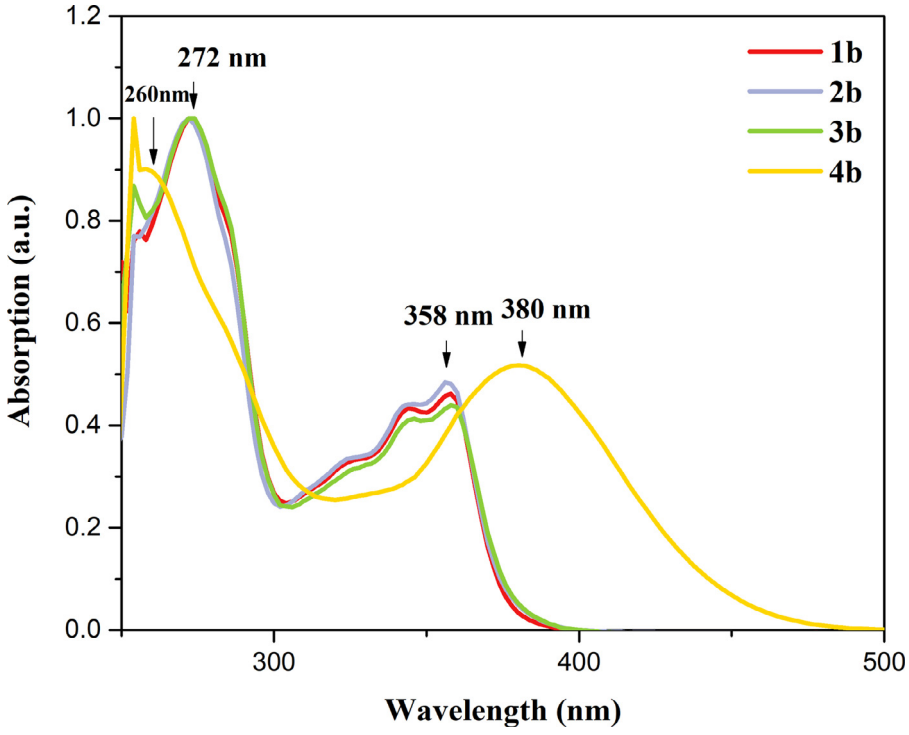

Fig. 4. Cytotoxic concentration (IC_{50}) of tested compounds 1–20 against (a) human lung cancer cell line (A549); (b) human hela cell line (HeLa); (c) human gastric carcinoma cell line (SGC-7901); (d) normal hepatocyte cell line (L02) by the MTT assay.

Table 2
Cytotoxic concentration (IC_{50}) of tested compounds against human lung cancer cell line (A549), human hela cell line (HeLa), human gastric carcinoma cell line (SGC-7901), normal hepatocyte cell line (L02) and by the MTT assay [63,64].

Compounds			IC_{50}			
	R^1	R^2	A549	Hela	SGC-7901	L-02
1a	CH_2CH_2Ph	–	31±6.25	73±6.55	>120	>200
1b	CH_2CH_2Ph	CH_3	54±5.39	36±0.98	89±1.80	139±13.60
1c	CH_2CH_2Ph	CH_2CH_3	82±2.49	57±2.77	84±7.49	140±10.35
1d	CH_2CH_2Ph	$CH_2CH_2CH_3$	55±4.58	44±3.95	89±2.89	127±9.58
1e	CH_2CH_2Ph	$CH_2(CH_3)_2$	57±14.24	51±2.94	73±4.18	131±8.08
2a	$CH_2CH_2Ph(OCH_3)_2$	–	94±4.63	73±4.83	>120	>200
2b	$CH_2CH_2Ph(OCH_3)_2$	CH_3	>120	>120	114±1.81	>200
2c	$CH_2CH_2Ph(OCH_3)_2$	CH_2CH_3	>120	>120	>120	>200
2d	$CH_2CH_2Ph(OCH_3)_2$	$CH_2CH_2CH_3$	>120	>120	>120	>200
2e	$CH_2CH_2Ph(OCH_3)_2$	$CH_2(CH_3)_2$	>120	>120	>120	>200
3a	CH_2Ph	–	46±18.96	>120	>120	>200
3b	CH_2Ph	CH_3	49±5.42	30±2.06	74±4.99	125±9.67
3c	CH_2Ph	CH_2CH_3	59±7.95	35±0.87	110±2.52	131±7.10
3d	CH_2Ph	$CH_2CH_2CH_3$	38±7.32	39±1.82	92±2.76	121±15.18
3e	CH_2Ph	$CH_2(CH_3)_2$	90±3.21	68±4.96	>120	>200
4a	$PhOCH_2Ph$	–	17±0.95	>120	>120	>200
4b	$PhOCH_2Ph$	CH_3	47±8.39	45±14.13	85±11.62	124±8.45
4c	$PhOCH_2Ph$	CH_2CH_3	12±1.48	7 ± 0.48	29±5.79	13±1.41
4d	$PhOCH_2Ph$	$CH_2CH_2CH_3$	4 ± 0.88	4 ± 0.42	14±1.96	32±3.66
4e	$PhOCH_2Ph$	$CH_2(CH_3)_2$	5 ± 0.64	7 ± 1.05	17±0.41	54±4.88
5-FU	–	–	98±0.72	109±2.81	113±1.07	>200
MTX	–	–	60±9.14	107±1.97	84±7.47	185±13.10

and base DG 9 and base DA 13, with benzene ring substituent at 8-position and base DC 12. It also displayed ionic interactions between benzene ring and R 458 with between pyridine ring and amino acid residue E 477 in addition to π-π interaction of N-phenyl ring with base DT 8 (Fig. 5b). Compound **1d** exhibited hydrogen bond donor interaction between N at 4-position and base DT 10. However, it displayed a similar low affinity score (−8.9 Kcal mol^{-1}) to docking mode of **1c**. It revealed three Ar-H interactions with bases DT 10, DA 13 and DT 8, besides π-π interactions between quinolone core and bases DG 9 and DC 12 in addition to ionic interaction of N-phenyl ring with amino acid residues K 417, D 437, R 458, respectively (Fig. 5c). In contrast, **1e** with an odd carbon number chain at N-1 position showed excellent inhibitory activity against S. aureus with affinity score −9.4 Kcal mol^{-1}. Its 3D ligand interaction revealed one hydrogen bond donor between the imine N and amino acid residue D 437 in addition to π-H

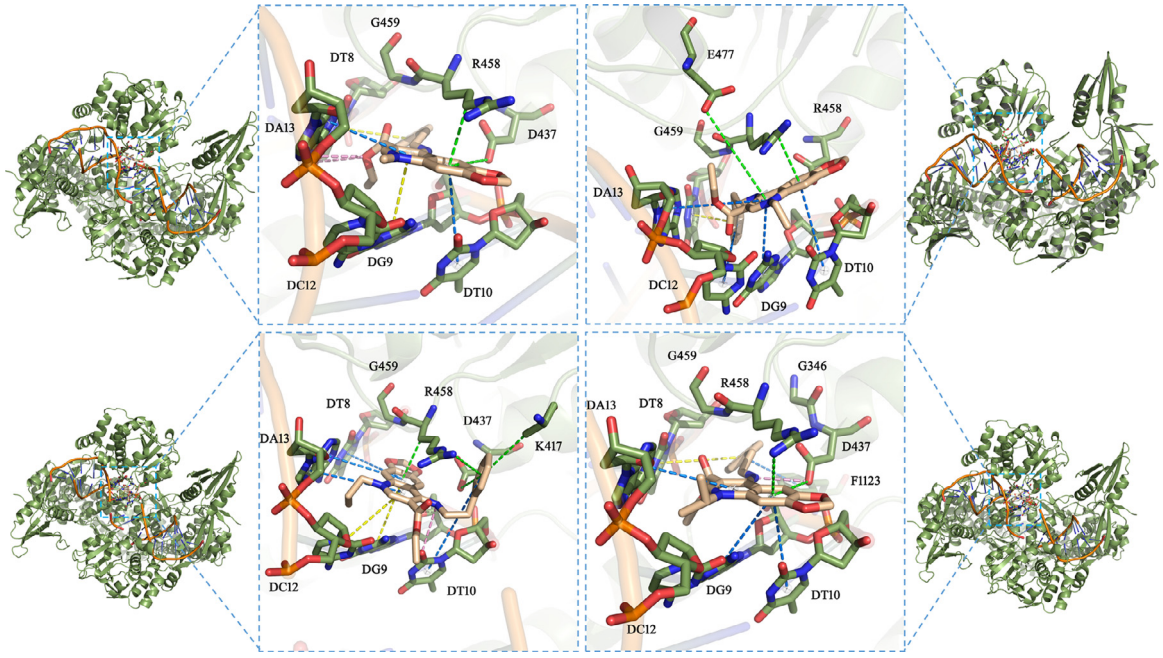

Fig. 5. The 3D binding mode of derivative $\mathbf{1_{b\text{-}e}}$ in the binding site of *S. aureus* DNA gyrase (Topo II, PDB ID: 2XCT). (a) Docking of compound **1b**; (b) Docking compound **1c**; (c) Docking of compound **1d**; (d) Docking of compound **1e**. ([H] Hydrogen Bonds are shown in pink and the yellow represents [π] π-π accumulation. Marine and gray represent [CH-π] π-H and hydrophobic bonds involved in amino acid bonding, respectively. [Cation-π/Anion-π] Ion-π bonds are colored in green).

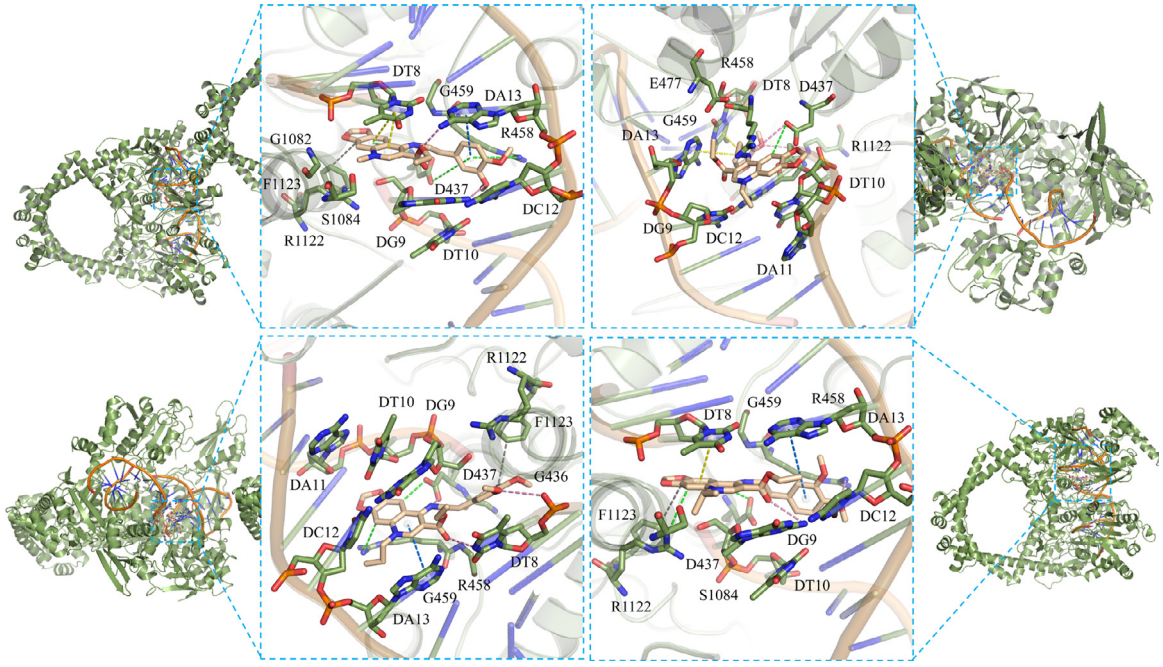

Fig. 6. The 3D binding mode of derivatives $\mathbf{2_{b\text{-}e}}$ in the binding site of *S. aureus* DNA gyrase (Topo II, PDB ID: 2XCT). (a) Docking of compound **2b**; (b) Docking compound **2c**; (c) Docking of compound **2d**; (d) Docking of compound **2e**. ([H] Hydrogen Bonds are shown in pink and the yellow represents [π] π-π accumulation. Marine and gray represent [CH-π] π-H and hydrophobic bonds involved in amino acid bonding, respectively. [Cation-π/Anion-π] Ion-Pi bonds are colored in green).

interactions of the quinoline ring also with base DT 10, DG 9, and DA 13, respectively, besides another π-H interaction between benzene ring introduced at position 8 with amino acid residue F 1123. And the spatial position of the compound at the binding site was very appropriate which would greatly be the cause of its good interactions and desired potency (Fig. 5d).

When the quinoline 4-position substituent is N-benzyl (**3a-e**), it is also fascinating to examine compounds with a long odd or even-numbered carbon substituent at 4-position of quinolone core. The docking mode of compound **3b** had an affinity score at −9.8 Kcal mol^{-1} (Fig. 7a). In the combined mode, the π-π interactions that occupied a large proportion between quinoline ring and bases DG 9, DC 12, and DA 13, respectively, played a major role. Moreover, π-π stacks also existed between benzene ring introduced at N-1 position and base DT 8. There was also a hydrogen bond receptor interaction between oxygen atom in dioxamol and base DC 12, which plays a role in determining the conformation direction of the entire structure in addition some other ion interactions and

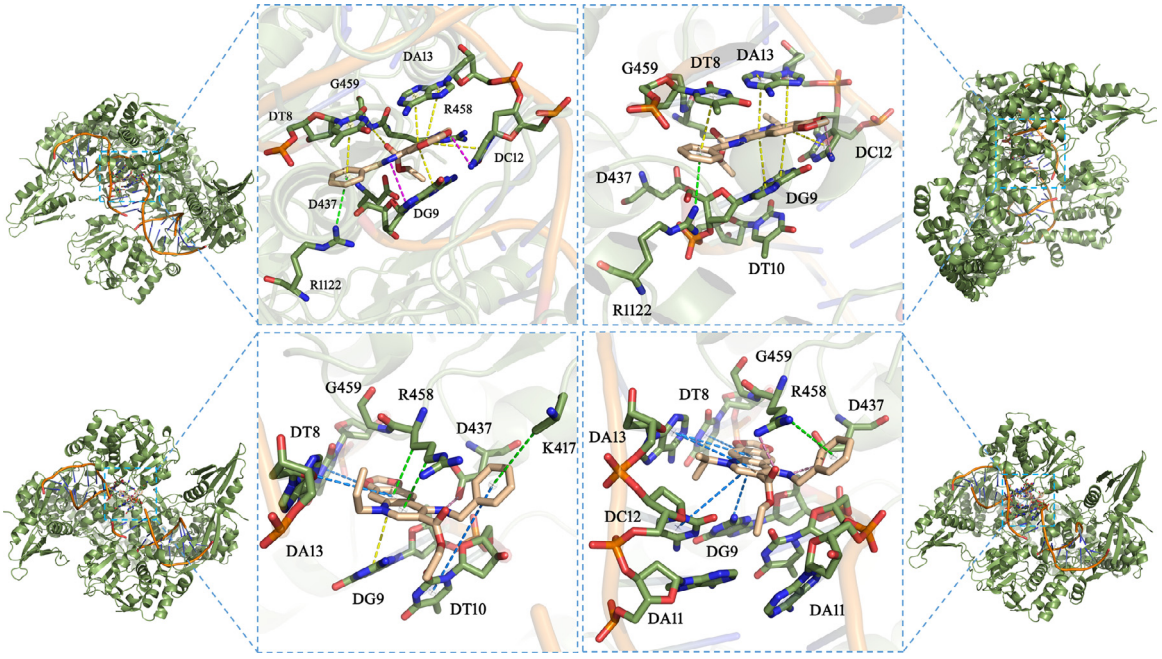

Fig. 7. The 3D binding mode of derivatives $\mathbf{3}_{\mathbf{b\text{-}e}}$ in the binding site of *S. aureus* DNA gyrase (Topo II, PDB ID: 2XCT). (a) Docking of compound **3b**; (b) Docking compound **3c**; (c) Docking of compound **3d**; (d) Docking of compound **3e**. ([H] Hydrogen Bonds are shown in pink and the yellow represents [π] π-π accumulation. Marine and gray represent [CH-π] π-H and hydrophobic bonds involved in amino acid bonding, respectively. [Cation-π/Anion-π] Ion-Pi bonds are colored in green).

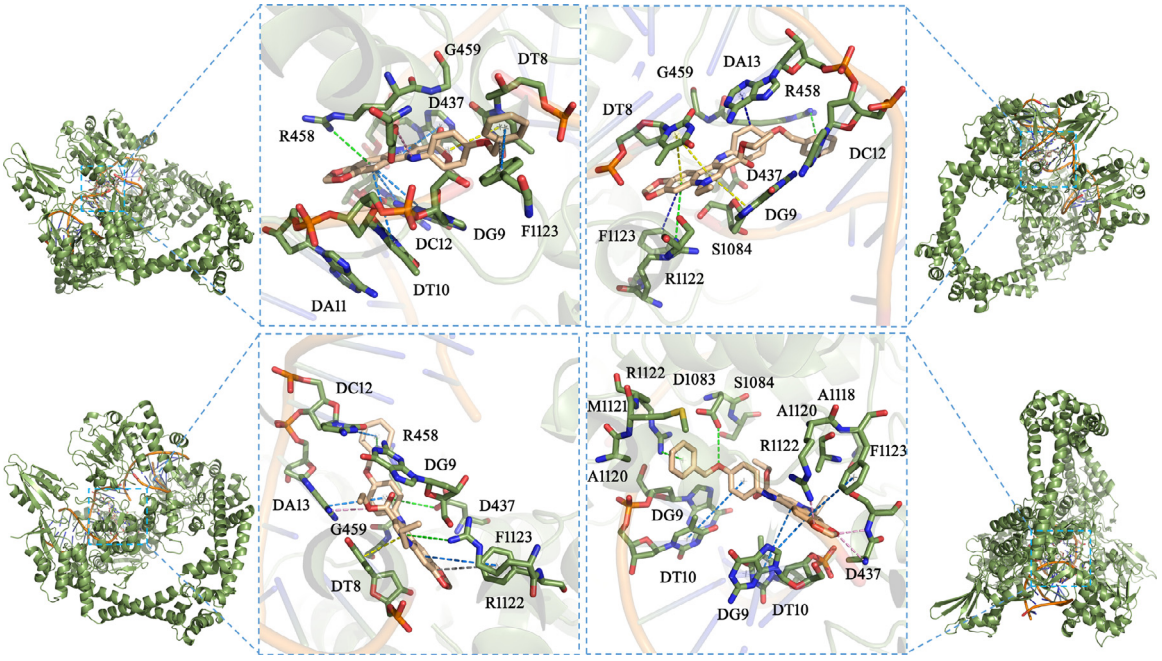

Fig. 8. The 3D binding mode of derivatives $\mathbf{4}_{\mathbf{b\text{-}e}}$ in the binding site of *S. aureus* DNA gyrase (Topo II, PDB ID: 2XCT). (a) Docking of compound **4b**; (b) Docking compound **4c**; (c) Docking of compound **4d**; (d) Docking of compound **4e**. ([H] Hydrogen Bonds are shown in pink and the yellow represents [π] π-π accumulation. Marine and gray represent [CH-π] π-H and hydrophobic bonds involved in amino acid bonding, respectively. [Cation-π/Anion-π] Ion-Pi bonds are colored in green).

van der Waals forces. As for the compound **3c** substituted with an even ethyl chain at the N-1 position, it showed a weaker effect consistent with the antibacterial activity (Fig. 7b). The oxygen atom at the 'bottom' of the compound is some 2.9 Å away from the DNA amine N of base DC 12, indicating that the oxygen atom is acting as an only O hydrogen-bond receptor. In this model, π-π interactions between compound and DNA bases takes up the main part of the force. In addition, there are other ionic and hydrophobic forces between the compound and the protein chain. According to the above, in the absence of CH-π fixation, it also lacks one hydrogen bond effect than the odd-chain-substituted compounds in the same series, which may prove its SAR simulation mechanism. Whereas the corresponding compounds **3d, 3e** perform well in biological activity, and the docking results contain two hydrogen

Table 3
Docking residues around the active pocket against *S. aureus* (PDBID: 2XCT).

Entry	Affinity score	Interaction with receptor					MIC
(PDBID 2XCT)	(kcal·mol^{-1})	[H]	π-H	π-π	Ion-Pi	Hydrophobic bond	*S. aureus*
1b	−9.9	DC12 DA13		DT8 DG9	R458 D437	DT10	12.5
1c	−8.7		DA13 DG9 DT10	DC12	R458 E477		25
1d	−8.9	DT10	DT8 DA13 DT10	DG9 DC12	R458 K417 D437		50
1e	−9.4	D437	DT10 DA13 DG9	DT8	R458	F1123	6.25
2b	−9.8	G459 D437	DA13	DT8	R458 D437	S1048	6.25
2c	−8.7	D437		DA13 R1122 G459	D437		25
2d	−9.3	DT8					
G459	DA13		R458 D437 K417	F1123	25		
2e	−9.8	DG9 R458	DA13	DT8	R1122 S1084	F1123	6.25
3b	−9.3	DC12 DG9		DA13 R458 DC12 DG9 DT8	R1122		12.5
3c	−9.3	DC12		DA13 DG9 DT8		R1122	25
3d	−9.0	D437	DT10 DT8		K417 R458		6.25
3e	−9.2	R458 DG9	DT8 DA13 DC12 DG9		R458		6.25
4b	−9.9	D437	F1122 DT10 DC12 DG9 D437	DT8	R458	F1122	3.125
4c	−9.2		DA13 F1123	DT8 DG9	R458 R1122		3.125
4d	−8.8	DA13	DA13 F1123 DC12	DT8	D437	R1122	3.125
4e	−8.9	R1122 D437	DG9 DT10 F1123		S1084 R1122		3.125

Table 4
Docking residues around the active pocket against *Human topoisomerase I* (PDBID: 1TL8).

PDBID	Entry	Affinity score (kcal·mol^{-1})	Interaction with receptor
1TL8	**1b**	−10.2	TPC11 DA13 DT10 Q633 H632 R488 R364 K532 I535
	1c	−9.8	TPC11 DT10 DG12 K532 K425
	1d	−9.7	TPC11 DA13 DT10 Q633 H632 R488 R364
	1e	−9.6	TPC11 DT10 DA112 K425 K532

bonding interactions, which may also be the mainly reason why these two odd-chain substituted compounds have outstanding activity (Fig. 7c, d). In addition, in compound **3d**, there are π-H interactions between the benzene ring and the bases DT 8 and DA 13, respectively, and this force also exists between the 8-substituted benzene ring base DT 10, besides some other ionic bonds. The action of compound **3e** also complements the antibacterial activity results, with the acceptor hydrogen bond between R 458 and carbonyl oxygen and the 4-position N and D 437 donor hydrogen bonds. Moreover, there are other CH-π interactions, which are between the quinoline parent ring and the bases DT 8, DA 13, DC 12 and DG 9, severally. Through the above, these molecular docking analyses find the most potent 2XCT inhibitors mechanism or mode for the prevention and treatment of infections caused by S. aureus (Table 3).

We also analyzed the anticancer activity and docked to simulate its mechanism of action. The target of its action is topoisomerase I, so the proteins we downloaded from the PDB database were processed after docking (PDBID: 1TL8). The docking found that the compounds with alkyl substituents were very close to the docking position and direction. In order to facilitate the explanation of the effect of the action force, we selected series 1 (compounds **1b**-**1e**) for comparison and explanation (Fig. 9, Table 4). Compound **1b** showed pleasant docking parameters, with a docking binding energy of −10.2 Kcal mol^{-1}, the highest in this series, which also masterly proved that the introduction of the quaternary ammonium salt iodomethyl side chain greatly improves the anticancer activity of the compound. There are multiple π-π stacking interactions between the pyridine ring of the compound and the base DT 105, between TPC 11 and the quinoline ring in the parent ring, and between the parent benzene ring and the base DA 113. At the same time, there are five ionic Pi bonds of the compound with amino acid Q 633, amino acid H 632, amino acid R 488, amino acid R 364 and amino acid K 532, respectively. In addition, there are some hydrophobic effects, for example, the N-benzyl substituent and the amino acid I 535 are tightly connected by the hydrophobic bond. These forces are the main representative forces of molecular simulation in this series. In contrast, compound **1d** with odd carbon number has almost the same spatial arrangement and spatial force as compound **1b** with affinity at −9.7 Kcal mol^{-1}. In addition to the lack of I535 hydrophobic bond, the simulation results are almost identical, which may be one of the reasons why its biological activity is slightly lower than that of **1b** (stronger than other in series 1). The affinity of compound **1e** with odd alkyl substituent chain is - 9.6 Kcal mol^{-1}, which is almost weaker than that of compound **1c** (−9.8 Kcal mol^{-1}). However, it was found that there is a reasonable hydrogen bond between TPC 11 and carbonyl oxygen except for some necessary π-π stacks. Finally, we analyzed the binding mode of compound **1c** and find that it was quite different in this group. First, its spatial distribution is very different from other similar compounds, and the amino acid distribution around it is also scarcely visible to the naked eye. Secondly, the binding of compound **1c** with 1Tl8 mainly depends on the π-π interactions between the pyridine and benzene ring of the parent core and TPC 11, between the base DT 10 and the pyridine ring, and between the N-benzyl substituent and the base DG 112, which seemed to be the same as the former compounds. However, the ion-Pi bonds that play the role of spatial positioning were very rare, only of com-

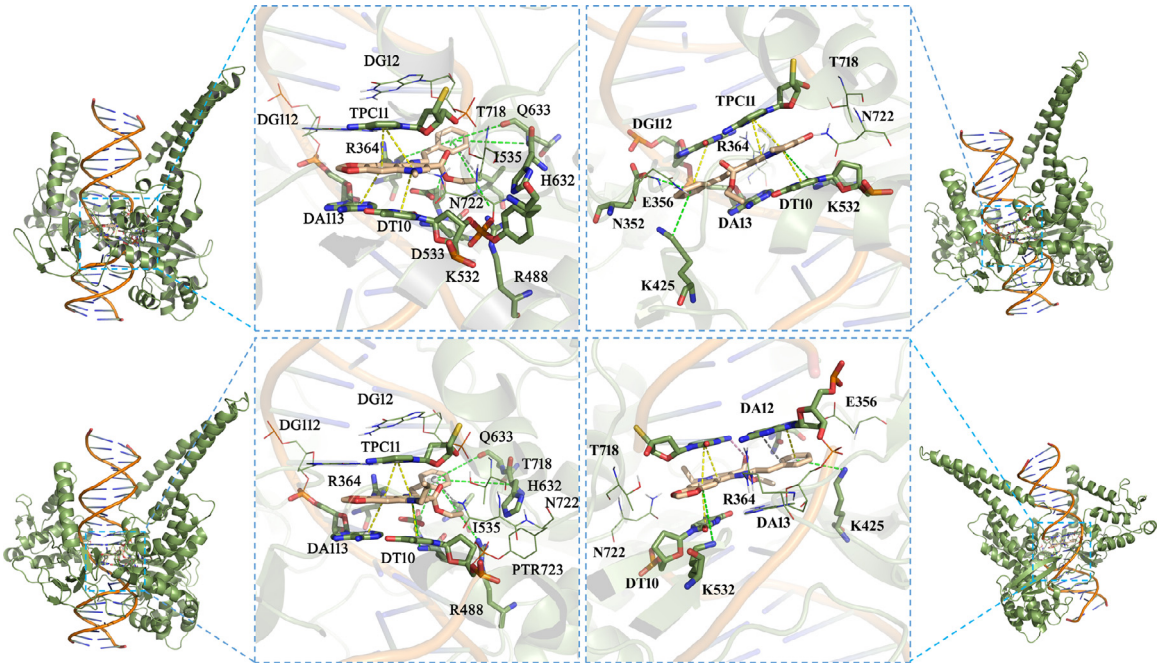

Fig. 9. The 3D binding mode of derivatives $\mathbf{1}_{\mathbf{b\text{-}e}}$ in the binding site of *Human topoisomerase I* (PDB ID: 1TL8). (a) Docking of compound **1b**; (b) Docking compound **1c**; (c) Docking of compound **1d**; (d) Docking of compound **1e**. ([H] Hydrogen Bonds are shown in pink and the yellow represents [π] π-π accumulation. Green and gray represent Ion-Pi interaction and Hydrophobic bonds involved in amino acid bonding, respectively).

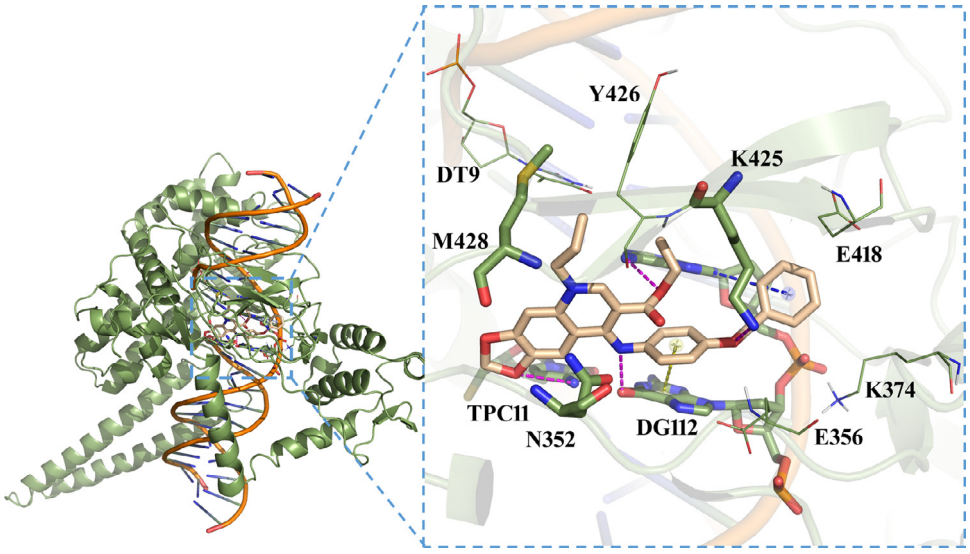

Fig. 10. The 3D binding mode of derivatives **4d** in the binding site of *Human topoisomerase I* (PDB ID: 1TL8). ([H] Hydrogen Bonds are shown in pink and the yellow represents [π] π-π accumulation. CH-Pi interaction involved in amino acid bonding is colored by marine).

pound with amino acid K 532 and amino acid K 425 have cation-Pi action, respectively, which may also be the reason for their weak action. And may also be listed as the reason for its poor anticancer activity to **1b** in the aspect of molecular docking.

According to the anticancer activity data, the activity of compound **4d** in the odd chain is the most prominent, so it is necessary to carry out targeted analysis of the compound. The docking of 4d displayed he binding affinity of −9.3 Kcal mol^{-1}(Figs. 10, 11). In the binding site of the enzyme displayed mainly hydrogen bond acceptor interactions through the oxygen of benzodioxoles with TPC 11, it also existed between the carbonyl oxygen and base DA 113, in addition between the oxygen of arylamine and amino acid residue K 425, and hydrogen bond donor interaction between the N at the 4-position and base DG 112. The compound also displayed π-π interactions of arylamine-substituted group with DG 112, and CH-π interactions of arylamine-substituted group and base DA 113. It also displayed other hydrophobic and cation interactions. According to the above analysis, even if the activities of the odd or even alkyl side chains were different, it is undoubted that the substituted compounds have outstanding antitumor activity. The interactions and affinity scores of the compounds suggest that the target compounds can served as an antitumor drug against cancer cells.

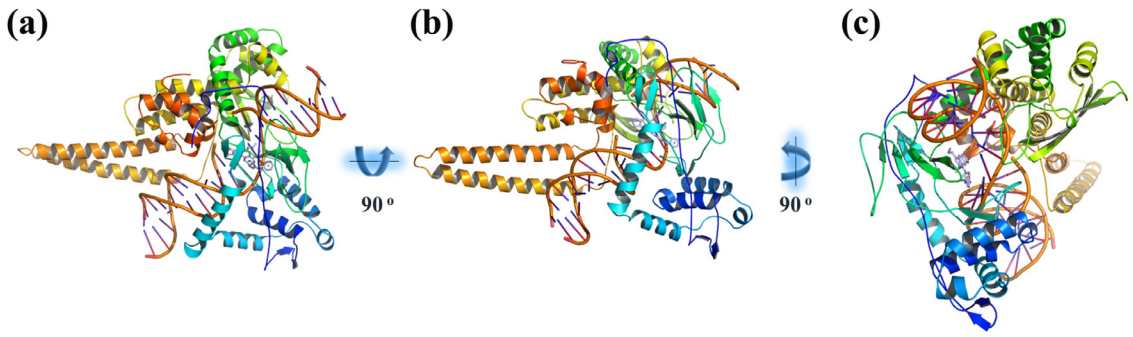

Fig. 11. Orthogonal views in two-dimensional spatial structure of 1Tl8–**4d** fusion protein. The active site of compound **4d** (lightblue, sticks) in DNA of protein. Molecular figures generated with Pymol 1.5.6 shown in publication type.

6. Conclusion

A summary of the common substitutions of several quinolone at the N-1 position was explored, and at the same time, the biological activity of the 20 compounds we synthesized with the odd and even carbon numbers of the alkyl side chain of the quaternary ammonium salt at the N-1 position were performed to explore the structure-activity relationship. The present study describes the design and bioactivities of twenty new quinoline derivatives as promising antimicrobial and antitumor agents based on DNA gyrase and DNA Topo I. Among the synthesized derivatives, twelve compounds (**1b, 1e, 2b, 2e, 3b, 3d, 3e, 4a, 4b, 4c, 4d**, and **4e**) showed promising antibacterial activities against tested *E. coli* and *S. aureus* bacterial strains more potent than amoxicillin and ciprofloxacin as reference. In the results of anticancer activity, compound **4d** showed very high antitumor activity, no matter in A549, SCG-7901, or HeLa cell line and become the most ideal dual active product. SAR study pointed out the importance of the 4-position substituted with hydrophobic phenyl rings and the N-1 position substituted with iodized salt to the antibacterial potency. Besides, the substitution of alkyl side chains with improved water solubility is a necessary condition for obtaining the best antibacterial and anticancer activity. In actual experiments, the cLog P value emphasizes its effect on the increase in the antibacterial activity of the quaternized ammonium products. In addition, docking study that substitution with odd carbon chain are essential for optimal antibacterial activities than even carbon chain (**1c, 2c, 3c**) and also discern the possible mechanism for their antibacterial potency. It revealed strong binding interactions in DNA gyrase active site on odd carbon chain and weak binding on even carbon chain. Anticancer activity docking in DNA Top I also revealed the possible mechanism of odd and even alkyl side chain activity, showing a clear difference in action. The study of N-1 substitution could lay a foundation for the follow-up study.

Declaration of Competing Interest

The authors declare that they have no known competing financial interests or personal relationships that could have appeared to influence the work reported in this paper.

CRediT authorship contribution statement

Yilin Wang: Conceptualization, Software. **Fuyan Xiao:** Data curation, Writing - original draft. **Guofan Jin:** Methodology, Supervision, Writing - review & editing.

Acknowledgement

This study was supported financially by the scientific research foundation of Jiangsu University (Grant no. 5501290005).

Supplementary materials

Supplementary material associated with this article can be found, in the online version, at doi:10.1016/j.molstruc.2020.128869.

References

[1] S.S. Bhagwat, M. Nandanwar, A. Kansagara, A. Patel, S. Takalkar, R. Chavan, H. Periasamy, R. Yeole, P.K. Deshpande, S. Bhavsar, A. Bhatia, J. Ahdal, R. Jain, M. Patel, Levonadifloxacin, a novel broad-spectrum anti-MRSA benzoquinolizine quinolone agent: review of current evidence, Drug Des. Dev. Therapy 13 (2019) 4351–4365, doi:10.2147/dddt.s229882.
[2] M. Neame, C. King, A. Riordan, A. Iyer, R. Kneen, I. Sinha, D.B. Hawcutt, Seizures and quinolone antibiotics in children: a systematic review of adverse events, Eur. J. Hosp. Pharm.-Sci. Pract. 27 (2020) 60–64, doi:10.1136/ejhpharm-2018-001805.
[3] D.C. Vieira, W.G. Lima, M.C. de Paiva, Plasmid-mediated quinolone resistance (PMQR) among Enterobacteriales in Latin America: a systematic review, Mol. Biol. Rep. 47 (2020) 1471–1483, doi:10.1007/s11033-019-05220-9.
[4] U. Acaroz, R. Dietrich, M. Knauer, E. Maertlbauer, Development of a generic enzyme-immunoassay for the detection of fluoro(quinolone)-Residues in Foodstuffs Based on a Highly Sensitive Monoclonal Antibody, Food Anal. Methods 13 (2020) 780–792, doi:10.1007/s12161-019-01695-1.
[5] S.L. Badshah, A. Ullah, New developments in non-quinolone-based antibiotics for the inhibiton of bacterial gyrase and topoisomerase IV, Eur. J. Med. Chem. 152 (2018) 393–400, doi:10.1016/j.ejmech.2018.04.059.
[6] F. Gao, P. Wang, H. Yang, Q. Miao, L. Ma, G. Lu, Recent developments of quinolone-based derivatives and their activities against Escherichia coli, Eur. J. Med. Chem. 157 (2018) 1223–1248, doi:10.1016/j.ejmech.2018.08.095.
[7] Q. Song, Z. Xu, H. Gao, D. Zhang, Overview of the development of quinolone resistance in Salmonella species in China, 2005-2016, Infect Drug Resist 11 (2018) 267–274, doi:10.2147/idr.s157460.
[8] I.V. Ukrainets, Y.V. Mospanova, N.L. Bereznyakova, A.A. Davidenko, Modification of the Benzene Moiety of the Quinolone Nucleus of 4-Hydroxy-6,7-dimethoxy-2-oxo-N-(pyridin-3-ylmethyl)- 1,2-dihydroquinoline-3-carboxamide as an Attempt to Enhance Its Analgesic Activity, Khimiko-farmatsevticheskii zhurnal 52 (2018) 8–12, doi:10.30906/0023-1134-2018-52-10-8-12.
[9] A. Li, J.W. Schertzer, X. Yong, Molecular conformation affects the interaction of the Pseudomonas quinolone signal with the bacterial outer membrane, J. Biol. Chem. 294 (2019) 1089–1094, doi:10.1074/jbc.AC118.006844.
[10] H. Nazik, G. Sass, S.R. Ansari, R. Ertekin, H. Haas, E. Deziel, D.A. Stevens, Novel intermicrobial molecular interaction: pseudomonas aeruginosa Quinolone Signal (PQS) modulates Aspergillus fumigatus response to iron, Microbiol.-Sgm 166 (2020) 44–55, doi:10.1099/mic.0.000858.
[11] H.M. Patel, D.P. Rajani, M.G. Sharma, H.G. Bhatt, Synthesis, molecular docking and biological evaluation of mannich products based on thiophene nucleus using ionic liquid, Lett Drug Des. Discov. 16 (2019) 119, doi:10.2174/1570180815666180502123743.
[12] H.M. Patel, K.D. Patel, H.D. Patel, Facile synthesis and biological evaluation of new mannich products as potential antibacterial, antifungal and antituberculosis agents: molecular docking study, Curr. Bioact. Compd. 13 (2017) 47–58, doi:10.2174/1573407212666160517145130.
[13] H.M. Patel, Synthesis of new mannich products bearing quinoline nucleous using reusable ionic liquid and antitubercular evaluation, Green Sustain. Chem. 5 (2015) 137, doi:10.4236/gsc.2015.54017.
[14] H.M. Patel, Current bioactive compounds synthesis, characterizations and microbial studies of novel mannich products using multicomponent reactions, 14 (2018) 278–288. 10.2174/1573407213666170424164716.
[15] Z. Ali, H. Ma, M.T. Rashid, A. Wali, S. Younas, Preliminary study to evaluate the phytochemicals and physiochemical properties in red and black date's vinegar, Food Sci. Nutr. 7 (2019) 1976–1985, doi:10.1002/fsn3.1009.
[16] H. Cui, M. Bai, Y. Sun, M.A.-S. Abdel-Sarnie, L. Lin, Antibacterial activity and mechanism of Chuzhou chrysanthemum essential oil, J. Funct. Foods 48 (2018) 159–166, doi:10.1016/j.jff.2018.07.021.

[17] P. He, G.-.L. Chen, S. Li, J. Wang, Y.-.F. Ma, Y.-.F. Pan, M. He, Evolution and functional analysis of odorant-binding proteins in three rice planthoppers: nilaparvata lugens, Sogatella furcifera, and Laodelphax striatellus, Pest. Manag. Sci. 75 (2019) 1606–1620, doi:10.1002/ps.5277.

[18] W. Hu, C. Li, J. Dai, H. Cui, L. Lin, Antibacterial activity and mechanism of Litsea cubeba essential oil against methicillin-resistant Staphylococcus aureus (MRSA), Ind. Crops Prod. 130 (2019) 34–41, doi:10.1016/j.indcrop.2018.12.078.

[19] Y. Liu, D. Zhang, G.-.M. Liu, Q. Chen, Z. Lu, Ameliorative effect of dieckol-enriched extraction from Laminaria japonica on hepatic steatosis induced by a high-fat diet via beta-oxidation pathway in ICR mice, J. Funct. Foods 58 (2019) 44–55, doi:10.1016/j.jff.2019.04.051.

[20] R. Lv, X. Huang, J.H. Aheto, C. Dai, X. Tian, Research on reaction mechanism of colorimetric sensor array with lead and its application for determination of lead content of fish, J. Food Process Eng. 42 (2019) e13075, doi:10.1111/jfpe.13075.

[21] M. Su, F. Liu, Z. Luo, H. Wu, X. Zhang, D. Wang, Y. Zhu, Z. Sun, W. Xu, Y. Miao, The antibacterial activity and mechanism of chlorogenic acid against foodborne pathogen pseudomonas aeruginosa, Foodborne Pathog. Dis. 16 (2019) 823–830, doi:10.1089/fpd.2019.2678.

[22] J. Xu, B. Wang, Y. Wang, Electromagnetic fields assisted blanching-Effect on the dielectric and physicochemical properties of cabbage, J. Food Process Eng. 42 (2019) e13294, doi:10.1111/jfpe.13294.

[23] Z. Zhang, M. Nie, C. Liu, N. Jiang, C. Liu, D. Li, Citrus flavanones enhance beta-carotene uptake in vitro experiment using caco-2 cell: structure-activity relationship and molecular mechanisms, J. Agric. Food Chem. 67 (2019) 4280–4288, doi:10.1021/acs.jafc.9b01376.

[24] L. Zhao, Y. Cheng, B. Li, X. Gu, X. Zhang, N.A.S. Boateng, H. Zhang, Integration of proteome and transcriptome data reveals the mechanism involved in controlling of Fusarium graminearum by Saccharomyces cerevisiae, J. Sci. Food Agric. 99 (2019) 5760–5770, doi:10.1002/jsfa.9844.

[25] Y. Zhao, X. Zhou, Y. Zhu, J. Zhang, Y. Dong, X. Xiao, Characterization and pulsed magnetic field inactivation of polyphenol oxidase from Jerusalem artichoke Nanyu 1, Food Sci. Nutr. 7 (2019) 4163-4163, doi:10.1002/fsn3.1189.

[26] R. Azargun, M.H.S. Barhaghi, H.S. Kafil, M.A. Oskouee, V. Sadeghi, M.Y. Memar, R. Ghotaslou, Frequency of DNA gyrase and topoisomerase IV mutations and plasmid-mediated quinolone resistance genes among Escherichia coli and Klebsiella pneumoniae isolated from urinary tract infections in Azerbaijan, Iran, J. Glob. Antimicrob. Resist. 17 (2019) 39–43, doi:10.1016/j.jgar.2018.11.003.

[27] K. Vinothkumar, S.R. Bhalara, A. Shah, T. Ramamurthy, S.K. Niyogi, G.N. Kumar, A.K. Bhardwaj, Involvement of topoisomerase mutations and qnr and aac(6')Ib-cr genes in conferring quinolone resistance to clinical isolates of Vibrio and Shigella spp. from Kolkata, India (1998-2009), J. Glob. Antimicrob. Resist. 13 (2018) 85–90, doi:10.1016/j.jgar.2017.10.013.

[28] D.H. Ki, F. Oppel, A.D. Durbin, A.T. Look, Mechanisms underlying synergy between DNA topoisomerase I-targeted drugs and mTOR kinase inhibitors in NF1-associated malignant peripheral nerve sheath tumors, Oncogene 38 (2019) 6585–6598, doi:10.1038/s41388-019-0965-5.

[29] R.M. Vala, D.M. Patel, M.G. Sharma, H.M. Patel, Impact of an aryl bulky group on a one-pot reaction of aldehyde with malononitrile and N-substituted 2-cyanoacetamide, RSC Adv. 9 (2019) 28886–28893, doi:10.1039/c9ra05975j.

[30] M.G. Sharma, R.M. Vala, D.M. Patel, I. Lagunes, M.X. Fernandes, J.M. Padron, V. Ramkumar, R.L. Gardas, H.M. Patel, Anti-Proliferative 1,4-Dihydropyridine and pyridine derivatives synthesized through a catalyst-free, one-pot multi-component reaction, ChemistrySelect 3 (2018) 12163, doi:10.1002/slct.201802537.

[31] H.M. Patel, Synthesis, characterizations and microbial studies of novel mannich products using multicomponent reactions, Curr. Bioact. Compd. 14 (2018) 278, doi:10.2174/1573407213666170424164716.

[32] S.S.R. Alsayed, S. Lun, G. Luna, C.C. Beh, A.D. Payne, N. Foster, W.R. Bishai, H. Gunosewoyo, Design, synthesis, and biological evaluation of novel arylcarboxamide derivatives as anti-tubercular agents, RSC Adv. 10 (2020) 7523–7540, doi:10.1039/c9ra10663d.

[33] L. Dinparast, S. Hemmati, A.A. Alizadeh, G. Zengin, H.S. Kafil, M.B. Bahadori, S. Dastmalchi, An efficient, catalyst-free, one-pot synthesis of 4H-chromene derivatives and investigating their biological activities and mode of interactions using molecular docking studies, J. Mol. Struct. 1203 (2020) 127426, doi:10.1016/j.molstruc.2019.127426.

[34] W. Xue, X. Li, G. Ma, H. Zhang, Y. Chen, J. Kirchmair, J. Xia, S. Wu, N-thiadiazole-4-hydroxy-2-quinolone-3-carboxamides bearing heteroaromatic rings as novel antibacterial agents: design, synthesis, biological evaluation and target identification, Eur. J. Med. Chem. 188 (2020) Unsp 112022, doi:10.1016/j.ejmech.2019.112022.

[35] T. Georgiev, Coronavirus disease 2019 (COVID-19) and anti-rheumatic drugs, Rheumatol. Int. 40 (2020) 825–826, doi:10.1007/s00296-020-04570-z.

[36] T.Y. Hu, M. Frieman, J. Wolfram, Insights from nanomedicine into chloroquine efficacy against COVID-19, Nat. Nanotechnol. 15 (2020) 247–249, doi:10.1038/s41565-020-0674-9.

[37] K. Kupferschmidt, J. Cohen, Race to find COVID-19 treatments accelerates, Science 367 (2020) 1412–1413, doi:10.1126/science.367.6485.1412.

[38] J. Bi, Y. Li, H. Wang, Y. Song, S. Cong, C. Yu, B.-.W. Zhu, M. Tan, Presence and formation mechanism of foodborne carbonaceous nanostructures from roasted pike eel (Muraenesox cinereus), J. Agric. Food Chem. 66 (2018) 2862–2869, doi:10.1021/acs.jafc.7b02303.

[39] M.G. Sharma, J. Pandya, D.M. Patel, R.M. Vala, V. Ramkumar, R. Subramanian, V.K. Gupta, R.L. Gardas, A. Dhanasekaran, H.M. Patel, One-Pot assembly for synthesis of 1,4-dihydropyridine scaffold and their biological applications, Polycycl. Aromat. Compd. 39 (2019) 395–485, doi:10.1080/10406638.2019.1686401.

[40] D.M. Patel, H.M. Patel, Trimethylglycine-betaine-based-catalyst-promoted novel and ecocompatible pseudo-four-component reaction for regioselective synthesis of functionalized 6,8-dihydro-1′H,5H-spiro[[1,3]dioxolo[4,5-g]quinoline-7,5′-pyrimidine]-2′,4′,6′(3′H)-trione derivativest, ACS Sustain. Chem. Eng. 7 (2019) 18667–18676, doi:10.1021/acssuschemeng.9b05184.

[41] D.M. Patel, R.M. Vala, M.G. Sharma, D.P. Rajani, H.M. Patel, A practical green visit to the functionalized [1,2,4]Triazolo[5,1-b]quinazolin-8(4H)one scaffolds using the group-assisted purification (GAP) chemistry and their pharmacological testing, Chemistryselect 4 (2019) 1031–1041, doi:10.1002/slct.201803605.

[42] D.M. Patel, M.G. Sharma, R.M. Vala, I. Lagunes, A. Puerta, J.M. Padron, D.P. Rajani, H.M. Patel, Hydroxyl alkyl ammonium ionic liquid assisted green and one-pot regioselective access to functionalized pyrazolodihydropyridine core and their pharmacological evaluation, Bioorg. Chem. 86 (2019) 137–150, doi:10.1016/j.bioorg.2019.01.029.

[43] H. Cui, C. Zhang, C. Li, L. Lin, Antibacterial mechanism of oregano essential oil, Ind. Crops Prod. 139 (2019) 111498 UNSP, doi:10.1016/j.indcrop.2019.111498.

[44] Y. Feng, Y. Zhu, J. Wan, X. Yang, C.K. Firempong, J. Yu, X. Xu, Enhanced oral bioavailability, reduced irritation and increased hypolipidemic activity of self-assembled capsaicin prodrug nanoparticles, J. Funct. Foods 44 (2018) 137–145, doi:10.1016/j.jff.2018.03.006.

[45] E. Fokum, H.M. Zabed, Q. Guo, J. Yun, M. Yang, H. Pang, Y. An, W. Li, X. Qi, Metabolic engineering of bacterial strains using CRISPR/Cas9 systems for biosynthesis of value-added products, Food Biosci. 28 (2019) 125–132, doi:10.1016/j.fbio.2019.01.003.

[46] R. Niu, Y. Yang, Y. Wang, S. Luo, C. Zhang, Y. Wang, Development and characterization of an immunoaffinity column for the detection of danofloxacin residues in milk samples, Food Sci. Technol. 39 (2019) 500–506, doi:10.1590/fst.34917.

[47] Y. Wen, J.-.H. Yuan, Q.-.Y. Zhou, W.-.B. Wang, X.-.F. Xu, Effect of broccoli extracts on proliferation inhibition and apoptosis in the colon SW620 Cells, Int. J. Agric. Biol. 22 (2019) 769–773, doi:10.17957/ijab/15.1128.

[48] H. Zhang, G.K. Mahunu, R. Castoria, Q. Yang, M.T. Apaliya, Recent developments in the enhancement of some postharvest biocontrol agents with unconventional chemicals compounds, Trends Food Sci. Technol. 78 (2018) 180–187, doi:10.1016/j.tifs.2018.06.002.

[49] W.-.D. Cai, W.-.Y. Qiu, Z.-.C. Ding, L.-.X. Wu, J.-.K. Yan, Conformational and rheological properties of a quaternary ammonium salt of curdlan, Food Chem. 280 (2019) 130–138, doi:10.1016/j.foodchem.2018.12.059.

[50] X.-.M. Chen, Z. Ma, D.D. Kitts, Effects of processing method and age of leaves on phytochemical profiles and bioactivity of coffee leaves, Food Chem. 249 (2018) 143–153, doi:10.1016/j.foodchem.2017.12.073.

[51] M. Elena Diaz-Casado, J.L. Quiles, E. Barriocanal-Casado, P. Gonzalez-Garcia, M. Battino, L.C. Lopez, A. Varela-Lopez, The paradox of coenzyme Q(10) in aging, Nutrients 11 (2019) 2221, doi:10.3390/nu11092221.

[52] L. Jiang, D. Wei, K. Zeng, J. Shao, F. Zhu, D. Du, An enhanced direct competitive immunoassay for the detection of kanamycin and tobramycin in milk using multienzyme-particle amplification, Food Anal. Methods 11 (2018) 2066–2075, doi:10.1007/s12161-018-1185-2.

[53] R. Osae, C. Zhou, W. Tchabo, B. Xu, E. Bonah, E.A. Alenyorege, H. Ma, Optimization of osmosonication pretreatment of ginger (Zingiber officinale Roscoe) using response surface methodology: effect on antioxidant activity, enzyme inactivation, phenolic compounds, and physical properties, J. Food Process Eng. 42 (2019) e13218, doi:10.1111/jfpe.13218.

[54] R. Osae, C. Zhou, B. Xu, W. Tchabo, H.E. Tahir, A.T. Mustapha, H. Ma, Effects of ultrasound, osmotic dehydration, and osmosonication pretreatments on bioactive compounds, chemical characterization, enzyme inactivation, color, and antioxidant activity of dried ginger slices, J. Food Biochem. 43 (2019) e12832, doi:10.1111/jfbc.12832.

[55] X. Ren, Q. Liang, H. Ma, Effects of sweeping frequency ultrasound pretreatment on the hydrolysis of zein: angiotensin-converting enzyme inhibitory activity and thermodynamics analysis, J. Food Sci. Technol.-Mysore 55 (2018) 4020–4027, doi:10.1007/s13197-018-3328-2.

[56] F. Sarpong, P. Oteng-Darko, M.K. Golly, L.P. Amenorfe, M.T. Rashid, C. Zhou, Comparative study of enzymes inactivation and browning pigmentation of apple (Malus domestica) slices by selected gums during low temperature storage, J. Food Biochem. 42 (2018) e12681, doi:10.1111/jfbc.12681.

[57] F. Sarpong, X. Yu, C. Zhou, H. Yang, B.B. Uzoejinwa, J. Bai, B. Wu, H. Ma, Influence of anti-browning agent pretreatment on drying kinetics, enzymes inactivation and other qualities of dried banana (Musa ssp.) under relative humidity-convective air dryer, J. Food Meas. Characterization 12 (2018) 1229–1241, doi:10.1007/s11694-018-9737-0.

[58] L. Wang, W. Li, Y. Liu, W. Zhi, J. Han, Y. Wang, L. Ni, Green separation of bromelain in food sample with high retention of enzyme activity using recyclable aqueous two-phase system containing a new synthesized thermo-responsive copolymer and salt, Food Chem. 282 (2019) 48–57, doi:10.1016/j.foodchem.2019.01.005.

[59] C. Zhang, H. Cui, Y. Han, F. Yu, X. Shi, Development of a biomimetic enzyme-linked immunosorbent assay based on molecularly imprinted polymers on paper for the detection of carbaryl, Food Chem. 240 (2018) 893–897, doi:10.1016/j.foodchem.2017.07.109.

[60] Y.-.Q. He, C.-.Y. Ma, Y. Pan, L.-.J. Yin, J. Zhou, Y. Duan, H. Zhang, H. Ma, Bioavailability of corn gluten meal hydrolysates and their effects on the immune system, Czech J. Food Sci. 36 (2018) 1–7, doi:10.17221/30/2017-cjfs.

[61] X. Jin, Q. Wang, X. Yang, M. Guo, W. Li, J. Shi, M. Adu-Frimpong, X. Xu, W. Deng, J. Yu, Chemical characterisation and hypolipidaemic effects of two purified Pleurotus eryngii polysaccharides, Int. J. Food Sci. Technol. 53 (2018) 2298–2307, doi:10.1111/ijfs.13821.

[62] X. Ren, Q. Liang, X. Zhang, T. Hou, S. Li, H. Ma, Stability and antioxidant activities of corn protein hydrolysates under simulated gastrointestinal digestion, Cereal Chem. 95 (2018) 760–769, doi:10.1002/cche.10092.
[63] G. Jin, F. Xiao, Z. Li, X. Qi, L. Zhao, X. Sun, Design, synthesis, and dual evaluation of quinoline and quinolinium iodide salt derivatives as potential anticancer and antibacterial agents, ChemMedChem 15 (2020) 600–609, doi:10.1002/cmdc.202000002.
[64] G. Jin, Z. Li, F. Xiao, X. Qi, X. Sun, Optimization of activity localization of quinoline derivatives: design, synthesis, and dual evaluation of biological activity for potential antitumor and antibacterial agents, Bioorg. Chem. 99 (2020) 103837, doi:10.1016/j.bioorg.2020.103837.